The Cryosphere Discuss., doi:10.5194/tc-2017-91, 2017
Manuscript under review for journal The Cryosphere
Discussion started: 31 May 2017

The Cryosphere Discussions
Open Access
EGU

Recent dynamic changes on Fleming Glacier after the disintegration of Wordie Ice Shelf, Antarctic Peninsula

Peter Friedl[1], Thorsten C. Seehaus[2], Anja Wendt[3], Matthias H. Braun[2], Kathrin Höppner[1]

[1]German Remote Sensing Data Centre (DFD), German Aerospace Centre (DLR), Oberpfaffenhofen, 82234, Germany
[2]Institute of Geography, Friedrich-Alexander-University Erlangen-Nuremberg, Erlangen, 91058, Germany
[3]Bavarian Academy of Sciences and Humanities, Munich, 80539, Germany

Correspondence to: Peter Friedl (peter.friedl@dlr.de)

Abstract. The Antarctic Peninsula is one of the world`s most affected regions by climate change. Several ice shelves retreated, thinned or completely disintegrated during recent decades, leading to acceleration and increased calving of their tributary glaciers. Wordie Ice Shelf, located at the south-western side of the Antarctic Peninsula, completely disintegrated in a series of events between the early 1970s and the late 1990s. We investigate the long-term response (1994–2016) of Fleming Glacier after the disintegration of Wordie Ice Shelf by analysing various multi-sensor remote sensing datasets. Our analysis reveals that after two decades of accelerated glacier flow and dynamic thinning the glacier tongue partially ungrounded between January and March 2008. From 2010 to 2011 a further phase of gradual grounding line recession was observed. In total, the retreat of the grounding line between 2008 and 2014 amounted to ~6–9 km and caused ~68 km^2 of the glacier tongue to go afloat. We attribute this to continuous dynamic thinning and pronounced basal melt at the grounding line, probably by a south-western Antarctic Peninsula wide oceanic warming. The bedrock topography revealed that a deep subglacial trough facilitated the grounding line retreat. In response to the ungrounding of the glacier tongue we observed an upstream propagation of high surface velocities. This resulted in a median speedup along the glacier`s centreline of ~1.4 m d^{-1} (~29 %) between 2007 and 2011. The propagation of acceleration has not yet affected regions far upstream (~50 km) of the glacier. Current ice thinning rates (2011–2014) in areas below 1000 m altitude range between ~2.6 to 3.1 m a^{-1} and are 60–70 % higher than between 2004 and 2008. Our study shows that Fleming Glacier is far away from approaching a new equilibrium and that the glacier dynamics are not primarily controlled by the loss of the ice shelf anymore. Currently, the tongue of Fleming Glacier is grounded in a zone of bedrock elevation of ~-400 m. However, about 3–4 km upstream modelled bedrock topography indicates a retrograde bed which transitions into a deep trough of up to -1000 m at ~10 km upstream. Hence, this endangers much larger ice masses in the future and a huge potential for an increase in sea level rise contribution.

1 Introduction

Recent studies have shown that the Antarctic Peninsula ice masses are strong contributors to sea level rise. In a consolidated effort Shepherd et al. (2012) estimated the contribution between 2005 and 2010 to 36 ± 10 Gt a^{-1} corresponding to 0.1 ± 0.03

mm a^{-1} SLE (sea level equivalent). This is considerably higher than their reported ice mass loss for the period from 1992 to 2000 of 8 ± 17 Gt a^{-1} (Shepherd et al., 2012). Huss and Farinotti (2014) computed from their ice thickness reconstruction of the northern and central Antarctic Peninsula a maximum potential sea level rise contribution of 69 ± 5 mm.

Rott et al. (2014) estimated the dynamic ice mass loss for the Larsen-A and B region after ice shelf disintegration to 4.21 ± 0.37 Gt a^{-1}. Seehaus et al. (2015; 2016) revealed similar values for tributary glaciers of the former Larsen-A and Prince-Gustav-Channel ice shelves. On the western Antarctic Peninsula south of 70° increased ice discharge and considerable thinning rates have been reported for various ice shelve tributaries (Wouters et al., 2015).

The main cause for the current increased ice discharge on the Antarctic Peninsula is the dynamic response of tributary glaciers to the disintegration and basal thinning of several ice shelves (e.g. Angelis and Skvarca, 2003; Pritchard et al., 2012; Rignot, 2006; Wouters et al., 2015; Wuite et al., 2015). With the reduction or loss of the buttressing effect of the ice shelves (Fürst et al., 2016; Mercer, 1978) due to thinning or disintegration, the tributary glaciers accelerate and show imbalance (Rignot et al., 2005; Rott et al., 2014; Scambos et al., 2004).

For the south-western Antarctic Peninsula Rignot et al. (2013) demonstrated that basal melt of ice shelves exceeded the ablation induced by calving. Wilkins Ice Shelf experienced amplified basal thinning due to small coastal atmospheric and oceanic processes that assist ventilation of the sub-ice-shelf cavity by upper-ocean water masses until ~8 years before break-up events took place in 2008 and 2009 (Braun and Humbert, 2009; Padman et al., 2012). Subsequent changes in ice dynamics and stresses leading to break-up have been observed (Rankl et al., 2016). On George VI Ice Shelf, surface lowering is linked to enhanced basal melt caused by an increased circulation of warmed Circumpolar Deep Water (CDW) (Holt et al., 2013) and a 13 % increase in ice flow was observed between 1992 and 2015 for its tributary glaciers (Hogg et al., 2017).

However, how the dynamic response after ice shelf loss progresses and how long this process lasts, is frequently unknown. Seehaus et al. (2016; 2017) showed that significant temporal differences in the adaptation of glacier dynamics in response to ice shelf decay can occur and that those can only be resolved, if dense time series of satellite-based measurements are available. Wendt et al. (2010) also concluded for Wordie Ice Shelf that its former tributaries were still far from reaching a new equilibrium after the retreat and collapse of the ice shelf starting in the 1960's. However, given the limited data used in previous studies, Wendt et al. (2010) pointed out that a much closer monitoring is required to verify this.

In this study we investigate the glacier dynamics of Fleming Glacier after the disintegration of Wordie Ice Shelf on the south-western Antarctic Peninsula. Our study ties in with previous works in the region, but covers a much longer time period at a much higher temporal resolution. We provide a time series of ice velocity measurements from Synthetic Aperture Radar (SAR) satellite data for the time period 1994–2016 for Fleming Glacier. In order to explain the observed changes in ice dynamics, we conducted an in-depth analysis of other geophysical and geodetic remote sensing data such as airborne Light Detection and Ranging (LiDAR) and satellite-borne laser altimetry, radio echo sounding for ice thickness, bistatic and monostatic SAR data as well as optical satellite images. We derive frontal retreat, surface velocity changes, ice elevation changes, grounding line positions and estimate the area of freely floating ice from hydrostatic equilibrium.

The Cryosphere Discuss., doi:10.5194/tc-2017-91, 2017
Manuscript under review for journal The Cryosphere
Discussion started: 31 May 2017

2 Study site

The former Wordie Ice Shelf was located in Marguerite Bay on the south-western Antarctic Peninsula. The ice shelf was originally fed by several major input units (Fig. 1). Among all former tributary glaciers, Fleming Glacier is the biggest. It has a current length of approx. 80 km and is up to 10 km wide at its tongue. With a speed of more than 8 m d^{-1} close to its calving front (Fig. 1), Fleming Glacier is also the fastest flowing glacier in Wordie Bay. Fleming Glacier merges with Seller and Airy Glacier ~8 km upstream of their joint calving front. Together with Rotz Glacier, which merges with Seller Glacier ~28 km upstream of the front, all four glaciers form the Airy-Rotz-Seller-Fleming glacier system, spanning a total catchment area of about 7000 km^2 (Cook et al., 2014).

Starting in the 1960s, Wordie Ice Shelf ran through a stepwise disintegration process (Fig. 1), which was controlled by pinning points (i.e. ice rises/rumples). Here the ice shelf was temporarily grounded and stabilized until the next rapid break up event took place (Doake and Vaughan, 1991; Reynolds, 1988; Vaughan, 1993; Vaughan and Doake, 1996). It is likely that the collapse of Wordie Ice Shelf was triggered by a combination of amplified ablation due to rising air temperatures (Doake and Vaughan, 1991), enhanced tidal action as a consequence of relaxed sea-ice conditions in Marguerite Bay (Reynolds, 1988) and increased basal melt rates on ice shelfs in the Bellingshausen Sea due to rising ocean temperatures (Holland et al., 2010; Pritchard et al., 2012; Rignot et al., 2013).

After the last big disintegration event in 1989, the ice shelf was split into a northern and a southern part (Doake and Vaughan, 1991). In the early 1990s most of the remaining floating ice in Wordie Bay consisted only of the protruding, unconfined tongues of the disconnected tributary glaciers. These tongues disappeared between 1998 and 1999, so that in 1999 Fleming Glacier was already calving near its 1996 grounding line (Rignot et al., 2005). Wendt et al. (2010) found the remaining area of floating ice to be only 96 km^2 in 2009. At this time there was virtually no contiguous ice shelf left and only the glaciers of the Prospect unit and Hariot`s unnamed neighbouring glacier still possessed floating glacier tongues (Wendt et al., 2010). During the following years (2010–2015) the fronts of the glaciers in Wordie Bay remained quite stable, except at the Prospect system where the once interconnected floating ice tongues of the three glaciers got disconnected and some floating ice got lost. This resulted in an total area of 84 km^2 of ice shelf in Wordie Bay in 2015, if taking the grounding line of 1996 as a baseline (Rignot et al., 2005; Rignot et al., 2011) and ignoring any grounding line migration.

While in the early 1990's an acceleration was not yet observed from the visual inspection of optical satellite imagery (Doake and Vaughan, 1991; Vaughan, 1993), Rignot et al. (2005) found substantial dynamic thinning and an increase of surface velocities by 40–50 % in 1996 against 3 point measurements by Doake (1975) in 1974 on Fleming Glacier (Fig. 1). The higher velocities as well as further thinning were also confirmed through Global Navigation Satellite System (GNSS) measurements in 2008 and airborne LiDAR surveys in 2004 and 2008 respectively (Wendt et al., 2010).

The Cryosphere Discuss., doi:10.5194/tc-2017-91, 2017
Manuscript under review for journal The Cryosphere
Discussion started: 31 May 2017

3 Data

We used a broad remote sensing data set in order to investigate the dynamic response of Fleming Glacier between 1994 and 2016 to the retreat and disintegration of Wordie Ice Shelf. Tab. 1 gives an overview of the specifications and the time coverages of the sensors used. The Bedmap2 digital elevation model (DEM) (Fretwell et al., 2013), resampled to 100 m resolution, was taken as a reference for geocoding and orthorectification of all SAR data products.

Calibrated and multi-looked SAR intensity images, Landsat 7 imagery and an existing dataset of ice shelf outlines (Ferrigno, 2008) were taken as a reference for the delineation of the ice shelf/glacier front (Tab. S1).

Calculations of elevation change rates were based on airborne LiDAR measurements, satellite-borne laser altimeter measurements and two DEMs derived from SAR interferometry (Tab. 1). The two DEMs covering the Airy-Rotz-Seller-Fleming glacier system were calculated from bistatic TerraSAR-X/TanDEM-X (TSX/TDX) Coregistered Single look Slant range Complex (CoSSC) strip map (SM) acquisitions on 2011-11-21 and monostatic TSX/TDX CoSSC SM acquisitions on 2014-11-03 (Fritz et al., 2012; Krieger et al., 2013). The TSX/TDX data were selected as close as possible to the dates of two NASA Operation IceBridge (OIB) Airborne Topographic Mapper (ATM) flights in 2011 and 2014, in order to be able to correct for radar penetration depth biases.

For the determination of the floating area on the tongue of Fleming Glacier, we used information on ice thickness and surface elevation from several Pre-IceBridge (PIB) and OIB flight lines across the Airy-Rotz-Seller-Fleming glacier system between 2002-11-26 and 2014-11-16 (Tab. 1). Depending on the date of acquisition, ice thickness data was recorded by different versions of the Coherent Radar Depth Sounder (CoRDS) (Tab. 1).

Our estimation of the recent grounding line of Fleming Glacier was based on a combination of the information on hydrostatic equilibrium with bedrock topography data, profiles of surface velocities and elevation change rate patterns inferred from the 2011–2014 TSX/TDX data. Information on bedrock topography was taken from the modelled bedrock grid of Huss and Farinotti (2014), which represents the most detailed dataset on bedrock topography available for the Antarctic Peninsula. However, although the Huss and Farinotti dataset reflects the general subglacial topography well, it has to be considered that its absolute bottom elevation values often differ by even more than 100 m from the OIB *CoRDS measurements.

4 Methods

4.1 Surface velocities

For each sensor consecutive pairs of coregistered single look complex SAR images were processed using an intensity offset tracking algorithm (Strozzi et al., 2002). A moving window was used to calculate surface displacements in azimuth and slant range direction between two SAR intensity images by localizing the peaks of an intensity-cross correlation function. The technique requires the definition of a tracking patch size and a step size (i.e. the distances in range and azimuth between the

centres of two consecutive moving windows, Tab. 1). The parameters were chosen according to the sensor specifications, the temporal baseline between the acquisitions and the expected displacement.

During the tracking procedure the implementation of a cross correlation threshold of 0.05 assured the removal of low quality offset estimates. Post-processing of the velocity fields comprises an additional filtering (Burgess et al., 2012) based on the comparison of the orientation and magnitude of the displacement vectors relative to their surrounding vectors. This algorithm discards over 90 % of unreasonable tracking results. The filtered displacement fields were then transferred from slant range geometry into ground range geometry, geocoded and orthorectified. The procedure to determine the error of the velocity measurements is described in the Supplemental material, Sect. S1. The errors for each velocity field are listed in Tab. S3.

4.2 Elevation change

We derived ice thinning rates on Fleming Glacier for 2004–2008 and 2011–2014 by subtracting ellipsoid heights of the PIB (ATM), the Centro de Estudios Científicos Airborne Mapping System (CAMS) and the OIB (ATM) airborne LiDAR datasets. Before subtraction, overlapping data of the originally closely spaced measurements were condensed to a common set of median surface elevations with an equal spacing of 50 m in along and across track direction. The locations of the resulting point clouds of differential elevation measurements are shown in Fig. 4. As described in Wendt et al. (2010) , we estimated the vertical accuracy of the measurements to be ± 0.2 m for all flights.

Additionally to the airborne LiDAR measurements ice elevation change rates for the period 2004–2008 were calculated from ellipsoid heights measured by the Ice, Cloud and Land Elevation Satellite (ICESat). Saturation of the 1064 nm Geoscience Laser Altimeter System (GLAS) detector can occur over ice, leading to a distorted echo waveform (Schutz et al., 2005). Hence we applied a saturation elevation correction provided on the GLA12 product prior to subtracting both tracks and excluded elevation measurements with flagged invalid saturation correction values from our analyses. Since both repeat tracks are not overlapping but separated by ~150 m in across track direction, we linearly interpolated the elevation data of the 2004 track onto the latitude values of the 2008 data prior to subtraction, similar to as described in Fricker and Padman (2006). In order to keep the error induced by interpolation low, elevation values were only allowed to be interpolated between two footprint centre locations with an along track spacing of ~170 m. This assured that existing gaps in the real data were preserved. Shuman et al. (2006) report a relative accuracy of ± 0.25 m for ICESat elevations measured on surface slopes between 1.5 and 2.0°. The mean surface slopes along the two ICESat elevation profiles were 1.9°. Hence, taking into account further possible inaccuracies of ± 0.15 m due to interpolation, we estimated the accuracy of the ICESat ice thinning rates to be ± 0.4 m.

A map of elevation change rates between 2011 and 2014 was calculated by differencing two TSX/TDX-DEMs. Both DEMs have a spatial resolution of 10 m. To generate the DEMs we applied a differential interferometric approach, which facilitates phase unwrapping by incorporating the topographic information of a reference DEM (Vijay and Braun, 2016). In order to stay consistent with the other SAR measurements, the resampled Bedmap2 DEM was chosen to be the reference DEM.

Before differencing, the TSX/TDX-DEMs must be vertically referenced to each other. For this purpose the median vertical offset between the DEMs was measured on preferably ice berg free areas of sea ice (Fig. S1), before one of the DEMs was adjusted accordingly. Neglecting differences in sea ice thickness, we corrected the amount of vertical adjustment for differences in tide level between the dates of the SAR acquisitions by using the TPXO8 tide model (Egbert and Erofeeva, 2002, updated). This model showed best performance for the prediction of tides in Antarctic seas (Stammer et al., 2014). After subtracting the vertically registered DEMs, the elevation differences were converted into yearly elevation change rates. We assessed the accuracy of the vertical registration over stable areas (i.e. tops of nunataks and rock outcrops, which were not affected by image distortions) at altitudes between 400 m and 1300 m (Fig. S1). The absolute median value of the extracted change rates was 0.43 m a^{-1} and accounts for errors related to the vertical registration and the tidal correction.

However, since radar signals can penetrate several meters into snow and ice, depending on the radar frequency and the dielectricity of the medium (Mätzler, 1987; Rignot et al., 2001), an additional bias is induced on glaciated areas when differencing interferometric DEMs from different times and/or frequencies (Berthier et al., 2016; Seehaus et al., 2015; Vijay and Braun, 2016). Since the TSX/TDX data was acquired only 4–7 days apart from the ATM data, differences in elevation change rates between the two datasets can be primarily attributed to differences in penetration depth at the TSX/TDX acquisitions in 2011 and 2014 and remaining vertical registration errors. In order to compare the TSX/TDX data with the ATM data, we extracted the TSX/TDX elevation change rates at the locations of the differential OIB ATM measurements using a 25 m buffer and calculated the median for each point. Hypsometric reference values were taken from the resampled Bedmap2 DEM which we converted to ellipsoidal heights using the included geoid correction layer. The comparison between elevation change rates obtained from the 2011–2014 OIB ATM flights and the 2011–2014 TSX/TDX data after the vertical registration of the DEMs showed a systematic overestimation of mean ice thinning of up to 2 m a^{-1} for the TSX/TDX measurements (Fig. S4 a). However, the general trend of the elevation change rates fits well to those calculated from the LiDAR data. We corrected the TSX/TDX data with a local polynomial model based on the elevation change rate differences between the ATM and the TSX/TDX data (Fig. S4 b). We applied this correction to all glaciated areas below 1000 m and clipped the TSX/TDX elevation change rate map accordingly. The RMSE between the cubic fits of the ATM elevation change rates and the extracted values from the corrected TSX/TDX map was 0.02 m (Fig. S4 c). However, by taking into account unknown errors due to the extrapolation of the correction factors to the entire glacier area, we assumed a remaining error of ± 0.2 m a^{-1} related to penetration depth differences. Together with the error of vertical registration and tidal correction, this resulted in a total error of ± 0.63 m a^{-1} for the TSX/TDX ice thinning rates.

For our analyses of elevation change we compared ice thinning rates from the PIB and the CECS airborne laser altimeter data (2004–2008) with rates obtained from the OIB data (2011–2014) as well as elevation change rates from the TSX/TDX data (2011–2014) with those derived from ICESat in 2004 and 2008. For the comparison between the TSX/TDX and the ICESat data, ice thinning rates were extracted from the TSX/TDX map at the GLAS centre locations of the 2008-10-04 track. To take into account the 70 m footprint of the GLAS instrument, we applied a buffer of 35 m and calculated the median from the extracted values at each point.

The Cryosphere Discuss., doi:10.5194/tc-2017-91, 2017
Manuscript under review for journal The Cryosphere
Discussion started: 31 May 2017

4.3 Floating area (hydrostatic height anomalies) and estimation of recent grounding line

In order to determine the floating area on the tongue of the Airy-Rotz-Seller-Fleming glacier system at different points in time, we derived hydrostatic height anomalies Δe from the PIB and OIB elevation and ice thickness measurements between 2002 and 2014. For every measuring point of ice thickness, Δe was calculated similar to Fricker (2002) by subtracting a theoretical freeboard height in hydrostatic equilibrium e_{he} from a measured orthometric ATM ice surface elevation e:

$$\Delta e = e - e_{he} \quad (1)$$

Regions on the glacier tongue where $\Delta e \approx 0$ were considered as freely floating. Before deriving hydrostatic height anomalies, we merged simultaneously acquired ice thickness and ATM data by calculating the median elevation within a buffer of 50 m at each ice thickness measurement. As the ATM heights were originally measured relative to the WGS84 ellipsoid, we converted the ellipsoidal ATM values to orthometric heights prior to the buoyancy calculations. For the conversion we used kriged geoid values calculated for a mean tide system with the EIGEN-6C4 global gravity field model (Förste et al., 2014). We calculated e_{he} by applying a modified formula after Griggs and Bamber (2011):

$$e_{he} = (H_i + \delta) - \frac{H_i \cdot \rho_i}{\rho_w} \quad (2)$$

where H_i is the measured PIB or OIB ice thickness, i.e. the ice thickness derived under the assumption that all ice is homogeneous and firn free, ρ_i is the ice density of pure ice, ρ_w is the density of sea water and δ is the firn density correction factor, i.e. the difference between the actual thickness of the firn layer above the glacier ice and the thickness that the firn would have if it were at the density of pure ice. Details on the uncertainties of all variables used for the calculations as well as the assessment of error propagation are provided in the Supplemental material, Sect. S2.

The buoyancy calculations provided information on the limit of hydrostatic equilibrium between 2002 and 2014 at several locations on the glacier system. As demonstrated in Seehaus et al. (2015), clear patterns of low or positive ice thinning rates in dh/dt maps reveal areas of floating ice, since buoyancy can cause originally grounded ice to bounce and/or mitigates the effect of ice thinning on ice surface elevation to ~10 %. Moreover, as basal friction is a major determent of surface velocities, velocity profiles can serve as additional information for locating the grounding line. Bedrock elevation data can reveal subglacial topographic features which act as pinning points for the glacier. Hence, our estimations of recent and previous grounding line positions was based on information on hydrostatic equilibrium from the hydrostatic height anomaly calculations as well as maps and profiles of TDX/TSX 2011–2014 elevation change rates, modelled bedrock topography (Huss and Farinotti, 2014) and surface velocities.

The Cryosphere Discuss., doi:10.5194/tc-2017-91, 2017
Manuscript under review for journal The Cryosphere
Discussion started: 31 May 2017

5 Results

5.1 Surface velocities

Figure 2 shows the multi sensor time series (1994–2016) of SAR intensity tracking derived velocities along a centreline profile on Fleming Glacier (Fig. 1). The profile extends from the grounding line location in 1996 to 16 km upstream. The relative distance of the glacier front to the 1996 grounding line is shown on the left side of the plot. Distances in the subsequent text are given in reference to the grounding line of 1996. Positive values relate to positions on the glacier upstream of (behind) the former grounding line while negative values refer to locations seawards of the 1996 grounding line.

After 1999 the glacier front remained comparatively stable close to the grounding line location in 1996 for almost 10 years. No obvious sign of velocity change is visible on our time series between the first measurements in 1994 and 2007. A comparison of the velocities on 1995-10-27 and 2007-10-23 (Fig. 3a) along the centreline profile reveals that the median velocity difference between 1995 and 2007 was just 0.04 m d^{-1}.

Between January and April 2008 a rapid acceleration of Fleming Glacier was noticeable along the centreline, which propagated ~8 km inland. Simultaneously, the front of Fleming Glacier retreated behind the 1996 grounding line for the first time. Although, since 2008 the glacier tongue never exceeded the 1996 grounding line anymore, the front remained quite stable. The velocity pattern persisted until March 2010, when a second phase of acceleration began. Our velocity time series shows that the acceleration gradually propagated further inland within one year, until it reached its final extension ~11 km upstream in early 2011. Between 2007-10-23 and 2011-10-02 the median increase in surface velocity along the profile was ~1.4 m d^{-1} or ~29 % (Fig. 3a, b). If ignoring velocity change in the vicinity of the 2011 glacier front, the highest relative acceleration values (~32–35 %) were recorded between ~7 and ~11 km upstream of the 1996 grounding line (Fig. 3b). The amount of relative acceleration rises significantly at ~7 km and abruptly drops at ~11 km. Peak absolute acceleration values of ~1.6 m d^{-1} were found at ~8 km. If excluding measurements in the region of frontal change between 2011 and 2015, no further marked changes in velocities could be detected along our centreline profile after 2011 (Fig. 3 a, b). Surface velocities on 2013-12-24 at the three measuring sites of Doake (1975) ~50 km upstream (Fig. 1) were very similar to those measured in 1996 and 2008. Furthermore, the flow directions in 2013 were like those in 2008 and 1974 (Tab. 2).

5.2 Elevation change

Figure 4 shows elevation change rates on the Airy-Rotz-Seller-Fleming glacier system for the period between 2011 and 2014. The entire area undergoes a considerable drawdown. On Fleming Glacier highest ice thinning rates of ~5 m a^{-1} were recorded in a zone extending from ~8 to ~14 km upstream. On Seller Glacier the ice loss exceeds even ~6 m a^{-1} at about 7 km upstream. In general ice thinning decreases towards higher altitudes. A tendency to lower negative or even positive elevation change rates could be observed on the lower parts of the joint Fleming and Seller glacier tongue. However the pattern was not as clear as on Airy Glacier, where a distinct area of positive elevation change could be detected.

Figures 5 a) and b) show comparisons of elevation change rates for the times prior to (2004–2008) and after the glacier acceleration (2011–2014). For the location of the data see Fig. 4. In Fig. 5 a) elevation change rates from PIB ATM-CAMS measurements (2004–2008) are plotted together with rates from ATM measurements in 2011 and 2014. The large scattering of the data is due to the highly crevassed glacier tongue. Fig. 5 b) shows ice thinning rates from ICESat tracks in 2004 and 2008 together with rates calculated from 2011–2014 TSX/TDX data. Note that the ATM and ICESat data refer to different profiles.

Figure 5 shows that prior to the speedup (2004–2008) Fleming Glacier was already affected by pronounced surface lowering. A clear trend of increasing ice thinning rates towards the glacier front is visible. During this time period the maximum negative elevation change rates could be found close to the 1996 grounding line. Here the cubic regression functions imply that the ice surface lowered at a maximum of 4.1 ± 0.2 m a^{-1} for the CAMS-ATM measurements and at 4.6 ± 0.4 m a^{-1} for the ICESat data. The median ice thinning rates measured during 2004–2008 for the cubic fits were 1.5 ± 0.2 m a^{-1} on the CAMS-ATM flightpath and 1.9 ± 0.4 m a^{-1} on the ICESat track. This shows that Fleming Glacier did not show any sign of reaching a new equilibrium even almost 20 years after the partial disintegration of the ice shelf in 1989.The OIB ATM and the TSX/TDX elevation change rates between 2011 and 2014 reveal a significant change in pattern for the time after the glacier flow acceleration. A tendency to lower ice thinning rates is present towards the glacier front and high negative elevation change rates can be found in a zone between 10 – 15 km upstream, with maximum ice losses of 4.1 ± 0.2 m a^{-1} for the ATM, and 3.8 ± 0.63 m a^{-1} for the TSX/TDX cubic regression functions. The median elevation change rates were -3.1 ± 0.63 m a^{-1} for the 2011-2014 TSX/TDX data, extracted along the ICESat track, and -2.6 ± 0.2 m a^{-1} on the 2011-2014 ATM flight path. Our data show an overall increase of median ice thinning of ~0.9–1.2 m a^{-1} or 60–70 % between the periods from 2004 to 2008 and from 2011 to 2014.

5.3 Floating area (hydrostatic height anomalies) and estimation of recent grounding line

Figure 6 depicts the results of the hydrostatic height anomaly calculations from PIB and OIB elevation and ice thickness data acquired before (2002–2004) and after the speedup of Fleming Glacier (2011–2014). Detailed plots showing the results of the hydrostatic height anomaly calculations along PIB and OIB flight lines can be found in the Supplemental Material, Fig. S5 a–e.

The hydrostatic height anomaly data of 2002 and 2004 clearly reveal that the ice inland of the 1996 grounding line was not floating at these times. However, the same calculations for data acquired in 2011 and 2014 as well as patterns of low and positive elevation change rates in the TSX/TDX 2011–2014 dh/dt map prove that a vast part of the formerly grounded glacier tongue had been freely floating after the final stage of glacier acceleration in 2011. In 2014 the estimated total freely floating area of the Airy-Rotz-Seller-Fleming glacier tongue was ~68 km^2.

The bedrock elevation model of Huss and Farinotti (2014) exhibits, that the boundary of the area showing flotation follows bedrock ridges. Those confine a subglacial trough underneath the Airy-Rotz-Seller-Fleming glacier system. The ridges are located several kilometres behind the 1996 grounding line. For most regions of the glacier tongue we estimate the current

grounding line to coincide with these ridges. We extracted data of surface velocities, TDX/TSX 2011–2014 elevation change rates, bedrock topography and if available hydrostatic height anomalies along four profiles on Airy and Fleming Glacier (Fig. 6). The plots suggest that after the first acceleration phase in 2008 the grounding line had not yet retreated as far as after the second acceleration phase between 2010 and 2011. For Seller Glacier no information on the 2008 grounding line position was deducible. For each profile possible and likely grounding line positions after the first acceleration in 2008 and today are shown in Fig. 6. The plots of the extracted data as well as more detailed information on the interpretation of the data in respect of the estimation of recent and previous grounding line positions are provided in the Supplemental Material, Fig. S6 1–4.

On the central part of Fleming Glacier velocities extracted along the centreline profile as well as along profile 3 (Fig. 6, Fig. S6 3) show that in 2011 high velocities had propagated upstream until to a chain of bedrock hills located up to 13 km upstream. However, hydrostatic height anomalies calculated from 2014 OIB data as well as the TSX/TDX elevation change rate map show no indication of ice floatation further upstream than ~6–9 km. This location is consistent with the propagation of high velocities in 2008 on the centreline profile and is estimated to be the likely recent grounding line position. A possible location of the grounding line after the initial ungrounding in 2008, however, is a gentle hill, ~2.5 km upstream of the grounding line in 1996.

6 Discussion

Our results confirm the previously detected acceleration of Fleming Glacier until 2007 after the stepwise break-up and disintegration of Wordie Ice Shelf (Rignot et al. 2005). No significant acceleration since 1996 could be found at the three measuring sites of Doake (1975) ~ 50 km glacier upstream, indicating that the recent speedup has not yet propagated until to these locations. Like Wendt et al. (2010), we also cannot confirm the change in flow direction in 1996 proposed by Rignot et al. (2005).

Abrupt speedups of tributary glaciers are often recorded as a direct consequence of loss of the buttressing force or major calving events (e.g. Seehaus et al., 2015). However, we did not observe any major calving event, which could have been responsible for the observed acceleration in 2008 or afterwards. The meltwater production on Fleming Glacier is considered to be generally not sufficient to percolate to the glacier bed (Rignot et al., 2005). Furthermore, a trend of cooling air temperatures is reported for the Antarctic Peninsula since the end of the 1990s (e.g. Turner et al., 2016), which likely further reduces surface melt. A possibly enhanced basal sliding as e.g. reported from Greenland (Moon et al., 2014) can hence be ruled out as explanation for the increase in flow velocities.

When ungrounding causes parts of the glacier tongue to go afloat, buttressing and basal friction is reduced. This in turn provokes the glacier to speed up and to dynamically thin. Rignot et al. (2002) demonstrated that if ungrounding occurs, the flow acceleration usually affects both the floating and the grounded part of the glacier, but is largest near the grounding zone. This is consistent with our observation of a highest relative speedup by ~32–35 % between 7 and 11 km upstream, which is

in the vicinity of our estimated recent grounding line location. Furthermore, 60–70 % higher ice thinning rates in the period between 2011 and 2014 point to an increased dynamic thinning in response to the grounding line retreat. The highest negative elevation change rates migrated upstream and can now be found in the vicinity of the estimated current grounding line. In the grounding zone basal melt adds to the dynamic thinning.

The bedrock topography reveals that the limits of hydrostatic equilibrium follow the edges of a subglacial trough underneath the joint Airy-Rotz-Seller-Fleming glacier tongue. We interpret this unfavourable bed topography to have promoted the grounding line retreat. Furthermore, before the speedup occurred, the highest ice thinning rates were recorded close to the grounding line position in 1996. This points to pronounced basal melt at the grounding line prior to the ungrounding. The bedrock topography of Fleming Glacier also shows a retrograde bed slope starting at ~3–4 km upstream of the current grounding line, which transitions into a pronounced deep trough (up to 1000 m below sea level) at about 10 km upstream. Hence, further thinning and subsequent ungrounding may have strong consequences and respective unstable conditions like on Twaites Glacier and in the Pine Island Bay region. Periodical pulses of warm CDW are known to flood onto the continental shelf of Marguerite Bay (Holland et al., 2010). Significant warming of Antarctic Continental Shelf Bottom Water (ASBW) of 0.1° to 0.3°C decade^{-1} since the 1990s were recorded in the Bellingshausen Sea region and linked to increased warming and shoaling of CDW (Schmidtko et al., 2014). The onset of Fleming Glacier`s speedup between January–March 2008 corresponds well with observations of Wouters et al. (2015). They reported first signs of a near simultaneous increase of ice mass loss for glaciers all across the western Antarctic Peninsula south of -70° since 2008 and an unabated rapid dynamic ice loss since 2009. In austral summer of 2007/2008 the lowest sea ice extent for the period 1978–2010 was recorded in the Bellingshausen/Amundsen Seas (Parkinson and Cavalieri, 2012). Wilkins Ice Shelf also showed various break-up events from beginning 2008 onwards after 10 years of absence of break-up events (Braun et al., 2009). Rankl et al. (2017) revealed a considerable speed-up of Wilkins Ice Shelf from 2007 to 2008. These tremendous changes were likely triggered by upwelling of relatively warm CDW which led to enhanced basal melt underneath of ice shelves as well as to a reduction of sea ice. Cook et al. (2016) proposed that oceanic melt induced by an increased shoaling of relatively warm CDW is the dominant driver for an accelerated frontal retreat of tidewater glaciers in the south-western Antarctic Peninsula since the 1990s. Other studies reported considerable thinning of the nearby George VI Ice Shelf (Hogg et al., 2017; Holt et al., 2013) and other ice shelves on the south-western Antarctic Peninsula (e.g. Rignot et al., 2013) due to increased basal melt. All in all, our observations show similarities with those made in the Amundsen Sea Sector, where the influx of relatively warm CDW onto the continental shelf is thought to be the dominant driver for recent substantial grounding line retreat, acceleration and dynamic thinning of several glaciers (Turner et al., 2017).

7 Conclusions

We presented a detailed history of the glacier dynamics of Fleming Glacier after the retreat and disintegration of Wordie Ice Shelf by analysing glacier extent, surfaces velocities, elevation change rates and hydrostatic equilibrium. Especially our

dense SAR time series enabled us to precisely date events of velocity change jointly with glacier retreat and elevation changes.

Our results show that until 2008 the dynamics of Fleming Glacier were primarily controlled by the impacts of break up events of Wordie Ice Shelf before the early 1990s. The retreat of the ice shelf reduced glacier buttressing and led to an increase in surface velocities, which in turn caused the glacier to dynamically thin. The last floating ice shelf parts were lost between 1998 and 1999. This showed no detectable effects on glacier flow dynamics.

After two decades of stable velocities, the glacier abruptly accelerated between January and April 2008 due to an ungrounding of the glacier tongue over extended areas. Further retreat of the grounding line between 2010 and 2011, an increase in surface velocities of ~29 % as well as 60–70 % higher ice thinning rates show that ungrounding in 2008 has initiated a new phase of dynamic instability. The unfavourable trough-shaped bed topography underneath Fleming Glacier amplified the grounding line retreat.

Our data suggest that enhanced basal melt at the grounding line due to increased shoaling of warm CDW most likely played a major role for the recent changes at Fleming Glacier. The ungrounding in 2008 coincides in time with accelerations of ice shelf tributary glaciers further in the south-west of the Antarctic Peninsula, break-up events and ice shelf speedup at Wilkins Ice Shelf as well as records of very low sea ice extent in the Bellingshausen and Amundsen Sea regions.

Today Fleming Glacier and the other glaciers of the Airy-Rotz-Seller-Fleming glacier system are far away of reaching a new equilibrium. The subglacial topography of Fleming Glacier upstream of the recent grounding line is characterized by some smaller landward deepening troughs which are separated by chains of gentle hills. As pronounced oceanic forcing is likely to continue, further retreat of the grounding line and more dynamic thinning are expected on Fleming Glacier. If the ungrounding would reach upstream to the retrograde bed slope at about ~3–4 km from the current grounding line and further to the deep subglacial trough, this could have fatal effects on the stability and sea level contribution of Fleming Glacier. However, on Airy and Seller glaciers the more favourable subglacial geometry of a landward steepening slope may slow down or prevent further grounding line retreat in the near future

Author contributions

Peter Friedl processed and analysed all SAR, optical, elevation and ground penetrating radar data. Thorsten C. Seehaus processed the ALOS PALSAR data and supported the interferometric DEM generation. Anja Wendt provided the CAMS LiDAR data and gave valuable comments. Matthias H. Braun coordinated the research and wrote the manuscript jointly with Peter Friedl. Kathrin Höppner initiated the project, co-coordinated the research in close cooperation with Matthias H. Braun and contributed to discussions of the results throughout. All authors revised the manuscript.

Competing interests

The authors declare no competing financial interests.

Acknowledgements

This project was mainly funded by the DLR VO-R Young Investigator Group “Antarctic Research”. Thorsten C. Seehaus was funded by Deutsche Forschungsgemeinschaft (DFG) in the framework of the priority program "Antarctic Research with comparative investigations in Arctic ice areas" by a grant to M.B. (BR 2105/9-1). Matthias H. Braun and Thorsten C. Seehaus would like to thank the HGF Alliance “Remote Sensing of Earth System Dynamics” (HA-310) and Marie-Curie-Network International Research Staff Exchange Scheme IMCONet (EU FP7-PEOPLE-2012-IRSES, Project Reference: 318718) for additional support. TerraSAR-X and TanDEM-X data were provided by DLR through the projects HYD3008 and XTI_GLAC7015. We would like to thank Rainer Lorenz (German Remote Sensing Data Centre, DLR) for his support retrieving the ERS-1/-2 SLC data from the ESA ERS-1/-2 Processing and Archiving Facility (D-PAF) at DLR and the ENVISAT ASAR SLC data from the ESA ENVISAT Processing and Archiving Centre (D-PAC) at DLR. Furthermore, we are grateful to Christian Kienholz (University of Alaska Fairbanks) and Bill Hauer (Alaska Satellite Facility) for providing the Radarsat-1 SLC data. Other remote sensing data was kindly made available by various institutions, e.g. ESA, NASA, JAXA, USGS and CReSIS. Finally, we would like to thank Paul Wachter and Saurabh Vijay for helpful comments.

References

Angelis, H. de and Skvarca, P.: Glacier surge after ice shelf collapse, Science (New York, N.Y.), 299, 1560–1562, doi: 10.1126/science.1077987, 2003.

Berthier, E., Cabot, V., Vincent, C. and Six, D.: Decadal Region-Wide and Glacier-Wide Mass Balances Derived from Multi-Temporal ASTER Satellite Digital Elevation Models. Validation over the Mont-Blanc Area, Front. Earth Sci., 4, 1103, doi: 10.3389/feart.2016.00063, 2016.

Braun, M. and Humbert, A.: Recent Retreat of Wilkins Ice Shelf Reveals New Insights in Ice Shelf Breakup Mechanisms, IEEE Geosci. Remote Sensing Lett., 6, 263–267, doi: 10.1109/LGRS.2008.2011925, 2009.

Burgess, E. W., Forster, R. R., Larsen, C. F. and Braun, M.: Surge dynamics on Bering Glacier, Alaska, in 2008–2011, The Cryosphere, 6, 1251–1262, doi: 10.5194/tc-6-1251-2012, 2012.

Cook, A. J., Holland, P. R., Meredith, M. P., Murray, T., Luckman, A. and Vaughan, D. G.: Ocean forcing of glacier retreat in the western Antarctic Peninsula, Science (New York, N.Y.), 353, 283–286, doi: 10.1126/science.aae0017, 2016.

Cook, A. J., Vaughan, D. G., Luckman, A. J. and Murray, T.: A new Antarctic Peninsula glacier basin inventory and observed area changes since the 1940s, Antarctic Science, 26, 614–624, doi: 10.1017/S0954102014000200, 2014.

Doake, C. S. M.: Bottom sliding of a glacier measured from the surface, Nature, 257, 780–782, doi: 10.1038/257780a0, 1975.

Doake, C. S. M. and Vaughan, D. G.: Rapid disintegration of the Wordie Ice Shelf in response to atmospheric warming, Nature, 350, 328–330, doi: 10.1038/350328a0, 1991.

Egbert, G. D. and Erofeeva, S. Y.: Efficient Inverse Modeling of Barotropic Ocean Tides, J. Atmos. Oceanic Technol., 19, 183–204, doi: 10.1175/1520-0426(2002)019<0183:EIMOBO>2.0.CO;2, 2002.

Ferrigno, J. G.: Coastal-change and glaciological map of the Larsen Ice Shelf area, Antarctica, 1940-2005, Reston, Va., 2008.

Förste, C., Bruinsma, S., Abrikosov, O., Lemoine, J.-M., Marty, J. C., Flechtner, F., Balmino, G., Barthelmes, F. and Biancale, R.: EIGEN-6C4 The latest combined global gravity field model including GOCE data up to degree and order 2190 of GFZ Potsdam and GRGS Toulouse, GFZ Data Services, 2014.

Fretwell, P., Pritchard, H. D., Vaughan, D. G., Bamber, J. L., Barrand, N. E., Bell, R., Bianchi, C., Bingham, R. G., Blankenship, D. D., Casassa, G., Catania, G., Callens, D., Conway, H., Cook, A. J., Corr, H. F. J., Damaske, D., Damm, V., Ferraccioli, F., Forsberg, R., Fujita, S., Gim, Y., Gogineni, P., Griggs, J. A., Hindmarsh, R. C. A., Holmlund, P., Holt, J. W., Jacobel, R. W., Jenkins, A., Jokat, W., Jordan, T., King, E. C., Kohler, J., Krabill, W., Riger-Kusk, M., Langley, K. A., Leitchenkov, G., Leuschen, C., Luyendyk, B. P., Matsuoka, K., Mouginot, J., Nitsche, F. O., Nogi, Y., Nost, O. A., Popov, S. V., Rignot, E., Rippin, D. M., Rivera, A., Roberts, J., Ross, N., Siegert, M. J., Smith, A. M., Steinhage, D., Studinger, M., Sun, B., Tinto, B. K., Welch, B. C., Wilson, D., Young, D. A., Xiangbin, C. and Zirizzotti, A.: Bedmap2: improved ice bed, surface and thickness datasets for Antarctica, The Cryosphere, 7, 375–393, doi: 10.5194/tc-7-375-2013, 2013.

Fricker, H. Amanda: Redefinition of the Amery Ice Shelf, East Antarctica, grounding zone, J. Geophys. Res., 107, doi: 10.1029/2001JB000383, 2002.

Fricker, H. Amanda and Padman, L.: Ice shelf grounding zone structure from ICESat laser altimetry, Geophys. Res. Lett., 33, doi: 10.1029/2006GL026907, 2006.

Fritz, T., Breit, H., Rossi, C., Balss, U., Lachaise, M. and Duque, S.: Interferometric processing and products of the TanDEM-X mission, Munich, Germany, 2012.

Fürst, J. Jakob, Durand, G., Gillet-Chaulet, F., Tavard, L., Rankl, M., Braun, M. and Gagliardini, O.: The safety band of Antarctic ice shelves, Nature Climate change, doi: 10.1038/nclimate2912, 2016.

Griggs, J. A. and Bamber, J. L.: Antarctic ice-shelf thickness from satellite radar altimetry, Journal of Glaciology, 57, 485–498, doi: 10.3189/002214311796905659, 2011.

Hogg, A. E., Shepherd, A., Cornford, S. L., Briggs, K. H., Gourmelen, N., Graham, J. A., Joughin, I., Mouginot, J., Nagler, T., Payne, A. J., Rignot, E. and Wuite, J.: Increased ice flow in Western Palmer Land linked to ocean melting, Geophys. Res. Lett., 353, 283, doi: 10.1002/2016GL072110, 2017.

Holland, P. R., Jenkins, A. and Holland, D. M.: Ice and ocean processes in the Bellingshausen Sea, Antarctica, J. Geophys. Res., 115, doi: 10.1029/2008JC005219, 2010.

Holt, T. O., Glasser, N. F., Quincey, D. J. and Siegfried, M. R.: Speedup and fracturing of George VI Ice Shelf, Antarctic Peninsula, The Cryosphere, 7, 797–816, doi: 10.5194/tc-7-797-2013, 2013.

Huss, M. and Farinotti, D.: A high-resolution bedrock map for the Antarctic Peninsula, The Cryosphere, 8, 1261–1273, doi: 10.5194/tc-8-1261-2014, 2014.

Krabill, W. B.: IceBridge ATM L1B Elevation and Return Strength, Version 2. [2011-11-17 - 2014-11-16], Boulder, Colorado USA, 2010, updated 2016.

Krabill, W. B.: Pre-IceBridge ATM L1B Qfit Elevation and Return Strength, Version 1. [2002-11-16, 2004-11-18], 2012.

Krieger, G., Zink, M., Bachmann, M., Bräutigam, B., Schulze, D., Martone, M., Rizzoli, P., Steinbrecher, U., Walter Antony, J., Zan, F. de, Hajnsek, I., Papathanassiou, K., Kugler, F., Rodriguez Cassola, M., Younis, M., Baumgartner, S., López-Dekker, P., Prats, P. and Moreira, A.: TanDEM-X: A radar interferometer with two formation-flying satellites, Acta Astronautica, 89, 83–98, doi: 10.1016/j.actaastro.2013.03.008, 2013.

Mätzler, C.: Applications of the interaction of microwaves with the natural snow cover, Remote Sensing Reviews, 2, 259–387, available at: http://www.tandfonline.com/doi/pdf/10.1080/02757258709532086, 1987.

Mercer, J. H.: West Antarctic ice sheet and CO2 greenhouse effect: a threat of disaster, Nature, 271, 321–325, doi: 10.1038/271321a0, 1978.

Moon, T., Joughin, I., Smith, B., Broeke, M. R., Berg, W. Jan, Noël, B. and Usher, M.: Distinct patterns of seasonal Greenland glacier velocity, Geophysical Research Letters, 41, 7209–7216, available at: http://onlinelibrary.wiley.com/doi/10.1002/2014GL061836/full, 2014.

Padman, L., Costa, D. P., Dinniman, M. S., Fricker, H. A., Goebel, M. E., Huckstadt, L. A., Humbert, A., Joughin, I., Lenaerts, Jan T. M., Ligtenberg, Stefan R. M., Scambos, T. and Van Den Broeke, Michiel R.: Oceanic controls on the mass balance of Wilkins Ice Shelf, Antarctica, J. Geophys. Res., 117, doi: 10.1029/2011JC007301, 2012.

Parkinson, C. L. and Cavalieri, D. J.: Antarctic sea ice variability and trends, 1979-2010, The Cryosphere, 6, 871–880, doi: 10.5194/tc-6-871-2012, 2012.

Pritchard, H. D., Ligtenberg, S R M, Fricker, H. A., Vaughan, D. G., van den Broeke, M R and Padman, L.: Antarctic ice-sheet loss driven by basal melting of ice shelves, Nature, 484, 502–505, doi: 10.1038/nature10968, 2012.

Rankl, M., Fürst, J. Jakob, Humbert, A. and Braun, M. Holger: Dynamic changes on Wilkins Ice Shelf during the 2006-2009 retreat derived from satellite observations, The Cryosphere Discuss., 1–17, doi: 10.5194/tc-2016-218, 2016.

Reynolds, J. M.: The structure of Wordie ice shelf, Antarctic peninsula, Bulletin-British Antarctic Survey, 57–64, 1988.

Rignot, E.: Changes in ice dynamics and mass balance of the Antarctic ice sheet, Philosophical transactions. Series A, Mathematical, physical, and engineering sciences, 364, 1637–1655, doi: 10.1098/rsta.2006.1793, 2006.

Rignot, E., Casassa, G., Gogineni, P., Kanagaratnam, P., Krabill, W., Pritchard, H. D., Rivera, A., Thomas, R., Turner, J. and Vaughan, D. G.: Recent ice loss from the Fleming and other glaciers, Wordie Bay, West Antarctic Peninsula, Geophys. Res. Lett., 32, doi: 10.1029/2004GL021947, 2005.

Rignot, E., Echelmeyer, K. and Krabill, W.: Penetration depth of interferometric synthetic-aperture radar signals in snow and ice, Geophys. Res. Lett., 28, 3501–3504, doi: 10.1029/2000GL012484, 2001.

Rignot, E., Jacobs, S., Mouginot, J. and Scheuchl, B.: Ice-shelf melting around Antarctica, Science (New York, N.Y.), 341, 266–270, doi: 10.1126/science.1235798, 2013.

Rignot, E., Mouginot, J. and Scheuchl, B.: Antarctic grounding line mapping from differential satellite radar interferometry, Geophys. Res. Lett., 38, n/a, doi: 10.1029/2011GL047109, 2011.

Rignot, E., Vaughan, D. G., Schmeltz, M., Dupont, T. and MacAyeal, D.: Acceleration of Pine Island and Thwaites Glaciers, West Antarctica, Annals of Glaciology, 34, 189–194, doi: 10.3189/172756402781817950, 2002.

Rott, H., Floricioiu, D., Wuite, J., Scheiblauer, S., Nagler, T. and Kern, M.: Mass changes of outlet glaciers along the Nordensjköld Coast, northern Antarctic Peninsula, based on TanDEM-X satellite measurements, Geophys. Res. Lett., 41, 8123–8129, doi: 10.1002/2014GL061613, 2014.

Scambos, T. A., Bohlander, J., Shuman, C. A. and Skvarca, P.: Glacier acceleration and thinning after ice shelf collapse in the Larsen B embayment, Antarctica, Geophys. Res. Lett., 31, doi: 10.1029/2004GL020670, 2004.

Schmidtko, S., Heywood, K. J., Thompson, A. F. and Aoki, S.: Multidecadal warming of Antarctic waters, Science, 346, 1227–1231, doi: 10.1126/science.1256117, 2014.

Schutz, B. E., Zwally, H. J., Shuman, C. A., Hancock, D. and DiMarzio, J. P.: Overview of the ICESat Mission, Geophys. Res. Lett., 32, doi: 10.1029/2005GL024009, 2005.

Seehaus, T., Cook, A., Silva, A. B. and Braun, M. H.: Changes in glacier dynamics at the northern Antarctic Peninsula since 1985, The Cryosphere Discuss., 1–31, doi: 10.5194/tc-2017-50, 2017.

Seehaus, T., Marinsek, S., Helm, V., Skvarca, P. and Braun, M.: Changes in ice dynamics, elevation and mass discharge of Dinsmoor–Bombardier–Edgeworth glacier system, Antarctic Peninsula, Earth and Planetary Science Letters, 427, 125–135, doi: 10.1016/j.epsl.2015.06.047, 2015.

Seehaus, T., Marinsek, S., Skvarca, P., van Wessem, J. M., Reijmer, C. H., Seco, J. L. and Braun, M. H.: Dynamic Response of Sjögren Inlet Glaciers, Antarctic Peninsula, to Ice Shelf Breakup Derived from Multi-Mission Remote Sensing Time Series, Front. Earth Sci., 4, F01005, doi: 10.3389/feart.2016.00066, 2016.

Shepherd, A., Ivins, E. R., A, G., Barletta, V. R., Bentley, M. J., Bettadpur, S., Briggs, K. H., Bromwich, D. H., Forsberg, R., Galin, N., Horwath, M., Jacobs, S., Joughin, I., King, M. A., Lenaerts, Jan T M, Li, J., Ligtenberg, Stefan R M, Luckman, A., Luthcke, S. B., McMillan, M., Meister, R., Milne, G., Mouginot, J., Muir, A., Nicolas, J. P., Paden, J., Payne, A. J., Pritchard, H., Rignot, E., Rott, H., Sørensen, L. Sandberg, Scambos, T. A., Scheuchl, B., Schrama, Ernst J O, Smith, B., Sundal, A. V., van Angelen, Jan H, van de Berg, Willem J, van den Broeke, Michiel R, Vaughan, D. G., Velicogna, I., Wahr, J., Whitehouse, P. L., Wingham, D. J., Yi, D., Young, D. and Zwally, H. Jay: A reconciled estimate of ice-sheet mass balance, Science (New York, N.Y.), 338, 1183–1189, doi: 10.1126/science.1228102, 2012.

Shuman, C. A., Zwally, H. J., Schutz, B. E., Brenner, A. C., DiMarzio, J. P., Suchdeo, V. P. and Fricker, H. A.: ICESat Antarctic elevation data. Preliminary precision and accuracy assessment, Geophys. Res. Lett., 33, doi: 10.1029/2005GL025227, 2006.

Stammer, D., Ray, R. D., Andersen, O. B., Arbic, B. K., Bosch, W., Carrère, L., Cheng, Y., Chinn, D. S., Dushaw, B. D., Egbert, G. D., Erofeeva, S. Y., Fok, H. S., Green, J. A. M., Griffiths, S., King, M. A., Lapin, V., Lemoine, F. G., Luthcke, S. B., Lyard, F., Morison, J., Müller, M., Padman, L., Richman, J. G., Shriver, J. F., Shum, C. K., Taguchi, E. and Yi, Y.: Accuracy assessment of global barotropic ocean tide models, Rev. Geophys., 52, 243–282, doi: 10.1002/2014RG000450, 2014.

Strozzi, T., Luckman, A., Murray, T., Wegmuller, U. and Werner, C. L.: Glacier motion estimation using SAR offset-tracking procedures, IEEE Trans. Geosci. Remote Sensing, 40, 2384–2391, doi: 10.1109/TGRS.2002.805079, 2002.

Turner, J., Lu, H., White, I., King, J. C., Phillips, T., Hosking, J. Scott, Bracegirdle, T. J., Marshall, G. J., Mulvaney, R. and Deb, P.: Absence of 21st century warming on Antarctic Peninsula consistent with natural variability, Nature, 535, 411–415, doi: 10.1038/nature18645, 2016.

Turner, J., Orr, A., Gudmundsson, G. Hilmar, Jenkins, A., Bingham, R. G., Hillenbrand, C.-D. and Bracegirdle, T. J.: Atmosphere-Ocean-Ice Interactions in the Amundsen Sea Embayment, West Antarctica, Rev. Geophys., doi: 10.1002/2016RG000532, 2017.

Vaughan, D. G.: Implications of the break-up of Wordie Ice Shelf, Antarctica for sea level, Antarctic Science, 5, doi: 10.1017/S0954102093000537, 1993.

Vaughan, D. G. and Doake, C. S. M.: Recent atmospheric warming and retreat of ice shelves on the Antarctic Peninsula, Nature, 379, 328–331, doi: 10.1038/379328a0, 1996.

Vijay, S. and Braun, M.: Elevation Change Rates of Glaciers in the Lahaul-Spiti (Western Himalaya, India) during 2000–2012 and 2012–2013, Remote Sensing, 8, 1038, doi: 10.3390/rs8121038, 2016.

Wendt, J., Rivera, A., Wendt, A., Bown, F., Zamora, R., Casassa, G. and Bravo, C.: Recent ice-surface-elevation changes of Fleming Glacier in response to the removal of the Wordie Ice Shelf, Antarctic Peninsula, Annals of Glaciology, 51, 97–102, doi: 10.3189/172756410791392727, 2010.

Wouters, B., Martin-Español, A., Helm, V., Flament, T., van Wessem, J M, Ligtenberg, S R M, van den Broeke, M R and Bamber, J. L.: Glacier mass loss. Dynamic thinning of glaciers on the Southern Antarctic Peninsula, Science (New York, N.Y.), 348, 899–903, doi: 10.1126/science.aaa5727, 2015.

Wuite, J., Rott, H., Hetzenecker, M., Floricioiu, D., Rydt, J. de, Gudmundsson, G. H., Nagler, T. and Kern, M.: Evolution of surface velocities and ice discharge of Larsen B outlet glaciers from 1995 to 2013, The Cryosphere, 9, 957–969, doi: 10.5194/tc-9-957-2015, 2015.

Zwally, H. J., Schutz, R., Bentley, C., Bufton, J., Herring, T., Minster, J., Spinhirne, J. and Thomas, R.: GLAS/ICESat L2 Antarctic and Greenland Ice Sheet Altimetry Data, Version 34, NASA National Snow and Ice Data Center Distributed Active Archive Center, Boulder, Colorado USA, 2014.

The Cryosphere Discuss., doi:10.5194/tc-2017-91, 2017
Manuscript under review for journal The Cryosphere
Discussion started: 31 May 2017

Figures

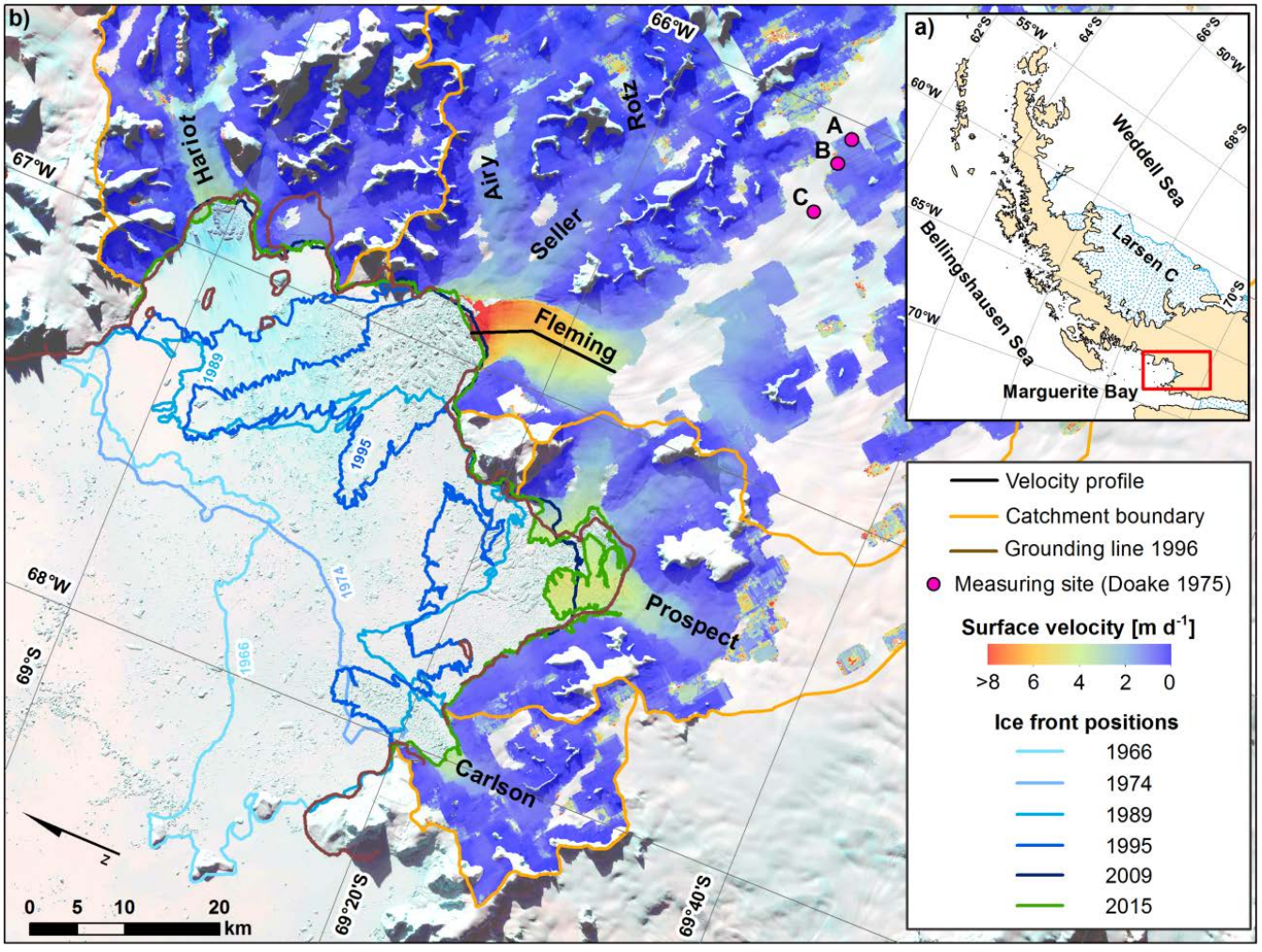

Figure 1: (a) Location of Wordie Bay at the Antarctic Peninsula. Map base: SCAR Antarctic Digital Database, version 6.0. **(b)** Surface velocity field and frontal positions of Wordie Ice Shelf between 1966 and 2015. Surface velocities were derived from Sentinel-1 acquisitions acquired on 28-08-2016 and 09-09-2015. Front positions (coloured lines) were taken from existing datasets or manually mapped from calibrated and multi-looked SAR intensity images. For detailed information on the data sources used for the frontal delineation see Supplemental material Tab. S1. The grounding line in 1996 (brown line) was derived from ERS-1/2 double difference interferometry (Rignot et al., 2005; Rignot et al., 2011). Black line: Extraction profile for the velocity time series presented in Sect. 5. Orange Line: Glacier system catchment boundaries from the SCAR Antarctic Digital Database, version 6.0. Pink dots: Sites of the velocity measurements undertaken by Doake, 1975 in 1974. Background: Mosaic of two Landsat-8 „Natural Colour“ images, acquired on 2015-09-16 ©USGS.

The Cryosphere Discuss., doi:10.5194/tc-2017-91, 2017
Manuscript under review for journal The Cryosphere
Discussion started: 31 May 2017

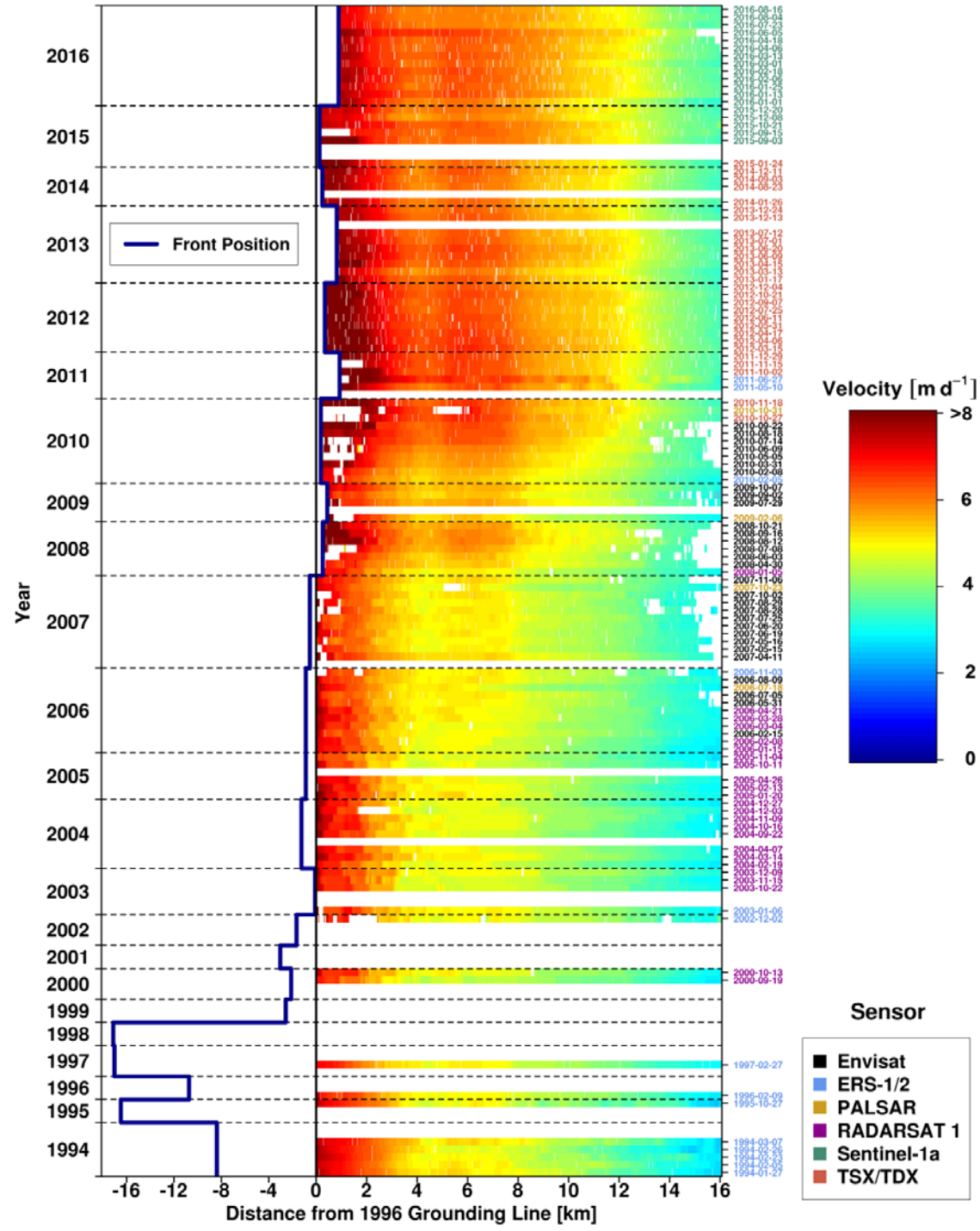

Figure 2: Left side: relative distance of the glacier front to the grounding line position in 1996. See Tab. S1 for data used for front mapping. Right side: velocity time series derived from multi sensor SAR intensity tracking along a centreline profile on Fleming Glacier starting at the 1996 grounding line (Fig. 1).

The Cryosphere Discuss., doi:10.5194/tc-2017-91, 2017
Manuscript under review for journal The Cryosphere
Discussion started: 31 May 2017

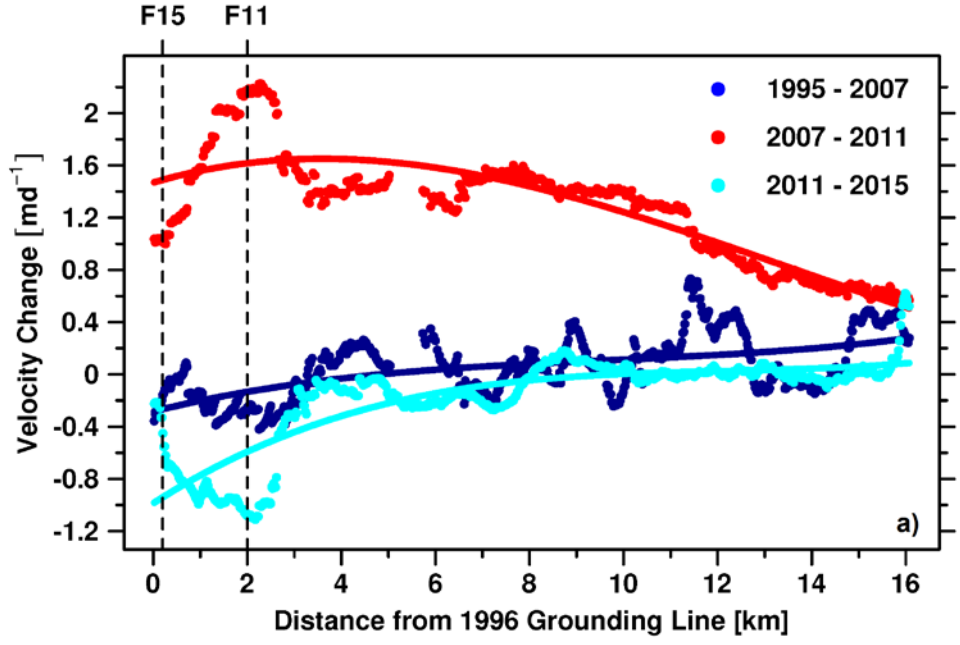

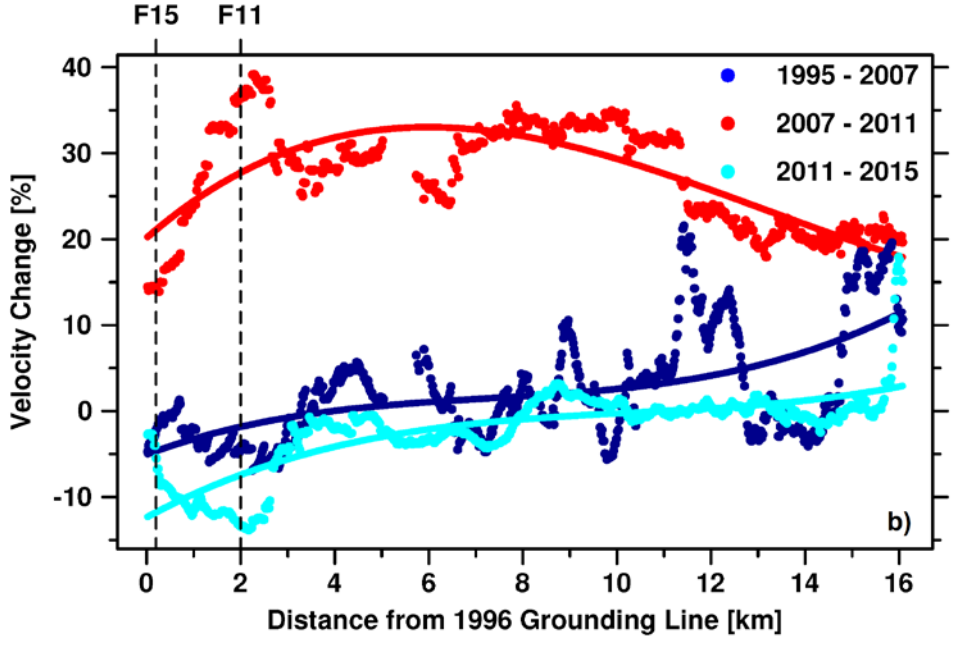

Figure 3: Absolute **(a)** and relative **(b)** velocity change along the centreline profile on Fleming Glacier (Fig. 1) for 1995-10-27 to 2007-10-23, 2007-10-23 to 2011-10-02 and 2011-10-02 to 2015-10-21. Coloured lines show cubic functions fitted to the data. F11: front position in 2011. F15: Front position in 2015. See Tab. S1 for data used for front mapping.

The Cryosphere Discuss., doi:10.5194/tc-2017-91, 2017
Manuscript under review for journal The Cryosphere
Discussion started: 31 May 2017

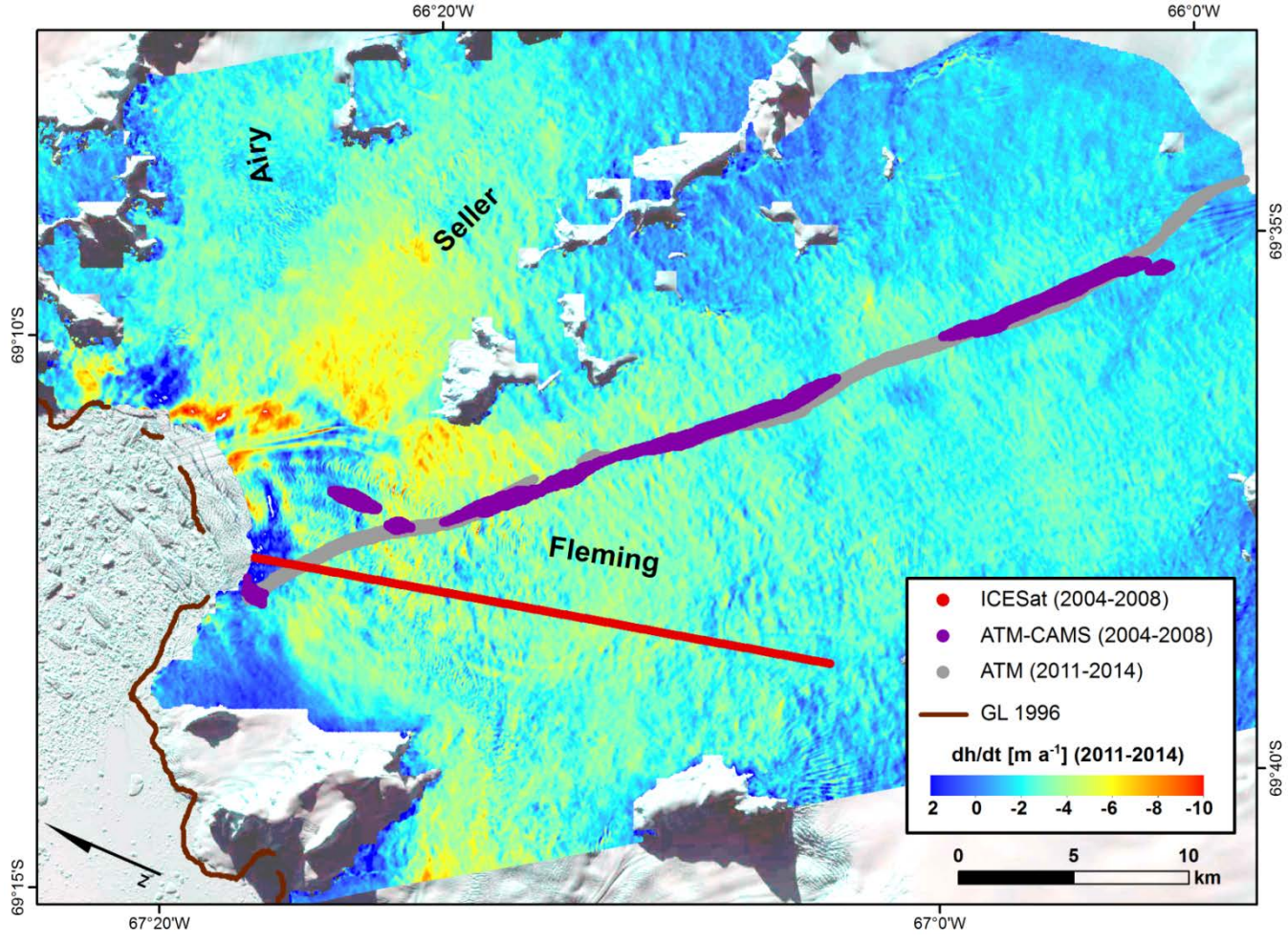

Figure 4: Glacier surface elevation change on Fleming Glacier between 2011 and 2014 derived from TSX/TDX bistatic and monostatic acquisitions. Red dots: ICESat track on 2008-10-04 taken as reference for ICESat 2004-2008 dh/dt calculations. Purple dots: common locations of PIB ATM and CAMS LiDAR measurements in 2004 and 2008. Grey dots: common locations of OIB ATM LiDAR measurements in 2011 and 2014. Brown line: grounding line in 1996 from Rignot et al. (2005) and Rignot et al. (2011). Background: Mosaic of two Landsat-8 „Natural Color" images, acquired on 2015-09-16 ©USGS.

The Cryosphere Discuss., doi:10.5194/tc-2017-91, 2017
Manuscript under review for journal The Cryosphere
Discussion started: 31 May 2017

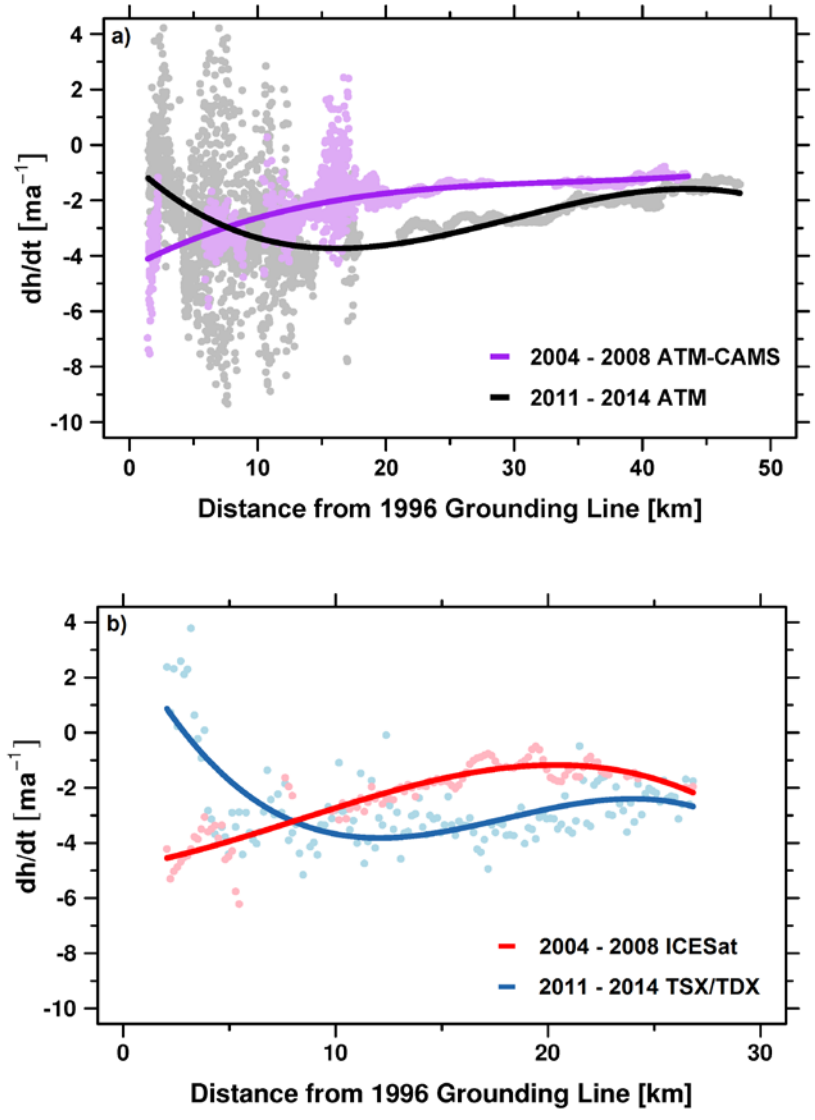

Figure 5: (a) Elevation change rates on Fleming Glacier 2004 – 2008 and 2011–2014 plotted against distance from the 1996 grounding line. Light purple dots: change rates from PIB ATM and CAMS LiDAR measurements in 2004 and 2008. Grey dots: change rates from OIB ATM LiDAR measurements in 2011 and 2014. See Fig. 4 for flight path locations. Purple and black lines: Cubic functions fitted to both datasets. **(b)** Elevation change rates on Fleming Glacier 2004–2008 and 2011–2014 plotted against distance from the 1996 grounding line. Light red dots: change rates from ICESat measurements in 2004 and 2008. Light blue dots: change rates between 2011 and 2014, extracted from the TSX/TDX dh/dt map along the 2008 ICESat track (see Fig. 4 for location). Red and blue lines: Cubic functions fitted to both datasets.

The Cryosphere Discuss., doi:10.5194/tc-2017-91, 2017
Manuscript under review for journal The Cryosphere
Discussion started: 31 May 2017

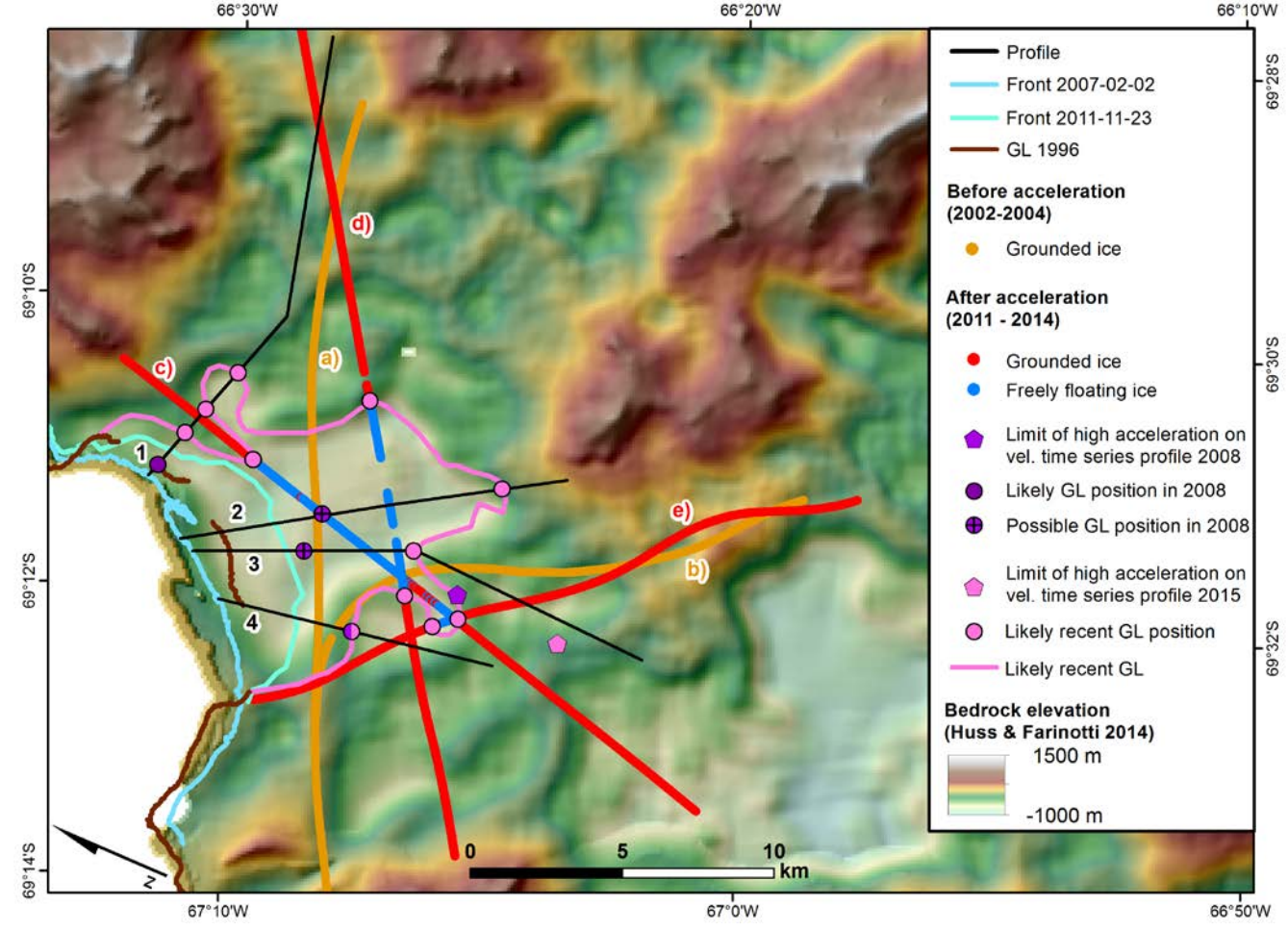

Figure 6: Floating area of Fleming Glacier and estimation of the recent grounding line. Black lines 1-4: Profiles for extraction of modeled bedrock elevations, surface velocities and elevation change rates (see Fig. S6 1–4). Light blue and cyan linens: glacier fronts on 2007-02-02 and 2011-11-23. Brown line: grounding line in 1996 (Rignot et al., 2005; Rignot et al., 2011). Orange dots: Fulfillment of floating condition before acceleration in 2008, derived from PIB LiDAR and ice thickness data. Dates of PIB flights: a) 2002-11-26, b) 2004-11-18. Background: bedrock elevation from Huss and Farinotti (2014). Blue and red dots: Fulfillment of the hydrostatic equilibrium assumption after the acceleration derived from OIB laser altimeter and ice thickness data. Dates of OIB flights: c) 2011-11-17, d) 2014-11-16, e) 2014-11-10. Purple pentagon: Location of the limit of high acceleration on the velocity time series profile in 2008 (Fig. 1 and 2). Purple circle: likely grounding line location in 2008. Purple circles with cross: possible grounding line locations in 2008. Pink pentagon: Location of the limit of acceleration on the velocity time series profile in 2015 (Fig. 1 and 2). Pink circles: Estimated positions of the recent grounding line obtained from buoyancy calculations, surface velocities, elevation change rate patterns and/or modeled bedrock elevations.

The Cryosphere Discuss., doi:10.5194/tc-2017-91, 2017
Manuscript under review for journal The Cryosphere
Discussion started: 31 May 2017

Tables

Table 1: Sensors and data used in this study and their main specifications. Intensity tracking parameters are provided in pixels [p] in slant range geometry.

SAR sensors

Platform	Sensor	Mode	SAR band	Repetition cycle [d]	Time interval [yyyy-mm-dd]	Tracking patch sizes [p x p]	Tracking step size [p x p]
ERS-1/2	AMI SAR	IM	C band	35/3/1	1994-01-26 2011-06-29	64x320	5x25
RADARSAT 1	SAR	ST	C band	24	2000-09-07 2008-01-17	128x512	5x20
Envisat	ASAR	IM	C band	35	2006-02-15 2010-10-10	64x320	5x25
ALOS	PALSAR	FBS	L band	46	2006-06-25 2010-11-23	128x384	10x30
TerraSAR-X/ TanDEM-X	SAR	SM	X band	11	2008-10-14 2015-01-30	512x512	25x25
Sentinel-1a	SAR	IW	C band	12	2015-08-28 2016-08-22	640x128	50x10

LiDAR/Laser Altimeter

Mission	Sensor	Type	Wavelength [nm]	Footprint [m]	Dates [yyyy-mm-dd]	Estimated accuracy	Reference
Pre-IceBridge (PIB)	ATM	LIDAR	532	1	2002-11-26 2004-11-18	0.20 m	Krabill (2012)
ICESat	GLAS	Laser Altimeter	1064	70	2004-05-18 2008-10-04	0.20 m	Zwally et al. (2014)
CECS/FACH	CAMS	LiDAR	900	1	2008-12-07	0.25 m	Wendt et al. (2010)
Operation IceBridge (OIB)	ATM	LiDAR	532	1	2011-11-17 2014-11-10 2014-11-16	0.20 m	Krabill (2010, updated 2016)

Ice Thickness

Mission	Sensor	Type	Bandwidth [MHz]	Sample spacing [m]	Dates [yyyy-mm-dd]
Pre-IceBridge (PIB)	ICoRDS-2	Radar	141.5-158.5	~130	2002-11-26
Pre-IceBridge (PIB)	ACoRDS	Radar	140-160	~30	2004-11-18
Operation IceBridge (OIB)	MCoRDS	Radar	180-210	~15	2011-11-17
Operation IceBridge (OIB)	MCoRDS 2	Radar	165-215	~15	2014-11-10 2014-11-16

The Cryosphere Discuss., doi:10.5194/tc-2017-91, 2017
Manuscript under review for journal The Cryosphere
Discussion started: 31 May 2017

Table 2: Comparison of surface velocities and flow directions at Fleming Glacier obtained by an optical survey in 1974 (Doake, 1975), SAR interferometry in 1996 (Rignot et al., 2005),GPS measurements in 2008 (Wendt et al., 2010) and SAR intensity tracking in 2013. Velocities and flow directions in 2013 were derived from intensity tracking applied on two TSX/TDX acquisitions on 2013-12-19 and 2013-12-30. For the locations of the measuring sites see Fig. 1.

Location	1974		1996		2008		2013	
	Magnitude m a^{-1}	Direction °	Magnitude m a^{-1}	Direction °	Magnitude m a^{-1}	Direction °	Magnitude m a^{-1}	Direction °
A (69.505° S, 66.049° W)	146 ± 4	277 ± 5	244 ± 10	285	205.5 ± 0.02	275.8 ± 0.1	205 ± 22	272
B (69.502° S, 66.123° W)	175 ± 4	272 ± 5	271 ± 10	287			244 ± 22	271
C (69.500° S, 66.267° W)	201 ± 4	283 ± 5	306 ± 10	300	312.8 ± 0.04	286.3 ± 0.1	323 ± 22	284

5